RSC Applied Interfaces

ROYAL SOCIETY OF CHEMISTRY

PAPER

View Article Online
View Journal | View Issue

Open Access Article. Published on 02 October 2024. Downloaded on 2/4/2026 5:17:06 AM.
This article is licensed under a Creative Commons Attribution-NonCommercial 3.0 Unported Licence.

Check for updates

Cite this: *RSC Appl. Interfaces*, 2024, **1**, 1436

Metal–organic frameworks as conductivity enhancers for all-solid-state lithium batteries†

Shruti Suriyakumar, [a] Rohit M. Manoj, [a] Sreelakshmy K. Jayaprakash,[a] Sreelakshmi Anil Kumar,[a] Keerthy P. Sudhakaran,[a] Vinesh Vijayan [b] and Manikoth M. Shaijumon *[ac]

Received 22nd July 2024,
Accepted 30th August 2024

DOI: 10.1039/d4lf00263f

rsc.li/RSCApplInter

Li-ion batteries are nonpareil when it comes to the combination of high energy and power density, making them the most suitable technology for electric vehicles, portable electronics and so on. Among Li-ion conductors, NASICON-type electrolytes are among the promising candidates for all-solid-state lithium batteries. However, the conventional synthesis approaches involve time-consuming multi-step high-temperature densification. Herein, we report a simple, efficient, and cost-effective strategy to develop composite solid electrolytes by incorporating MOFs in LATP using a powder cold press approach. Here, we report composite solid electrolytes (CSEs) composed of LATP ceramic particles and metal–organic frameworks (MOFs) in a SCN–LiTFSI matrix. The highly tunable porous structure of MOFs facilitates ion movement and acts as promising building materials for solid-state Li-ion conductors. In this study, the morphology, conductivity, and electrochemical cycling of LATP and its composite combinations are very well explored. Further, LATP–MOF composite solid electrolytes are tested for Li-ion and Li–Se batteries in an all-solid-state configuration with a lithium–metal anode.

Introduction

Throughout the last three decades, rechargeable lithium-ion batteries (LIBs) have been a reliable and dominant source of energy in portable electronics, large-scale energy storage devices and electric vehicles (EVs) due to their long-term cycling stability, high energy density and high operating potential.[1] However, using lithium metal alongside flammable organic liquid electrolytes also sums up the safety concern.[2] These two factors, increasing safety concerns and the pursuit of high energy densities, have energised the development of solid-state electrolytes (SEs). Solid-state batteries have excellent safety efficiency, high energy density, and a wide variety of operating temperatures, which are essential for EV applications. Also, by using solid electrolytes, it is possible to fabricate bipolar-stacked electrodes by coupling with electrolytes, thereby designing batteries with high output voltage, high energy density, and simple components.[3]

SEs can be made of diverse materials ranging from inorganics (oxides, sulfides, argyrodites) or polymers to composite-based electrolytes.[4,5] The interfaces between the different components are critical when designing solid-state battery cells. For improved contact between the electrodes and electrolyte, the operating temperature and pressure are very vital. Further, to achieve good ionic conductivity and to reduce grain boundary resistance, oxides and NASICON-type SEs require multi-step high-temperature sintering and densification. Though sulfides and argyrodites can be compressed at relatively lower temperatures and pressure, they react violently with moisture, leading to performance degradation. Polymers also tend to decompose and thus exhibit lower critical current density. Therefore, cold pressing the solid electrolyte powder with a suitable binder or framework is considered an alternative. There are reports on blending solid electrolytes with a spectrum of suitable binders like polytetrafluoroethylene (PTFE) and poly(vinylidene fluoride) (PVDF) and then using them as electrolytes post-pelletising.[6,7] For instance, embedding NASICON-type oxide, $Li_{1+x}Al_xTi_{2-x}(PO_4)_3$ (LATP), into a PVDF–HFP matrix and LATP with succinonitrile (SCN) and polyacrylonitrile as interlayers has been shown to improve the performance.[8] However, the binder persists as an inactive component and is redundant in terms of ionic conduction. Hence, a more effective strategy for balancing the electrochemical properties and the operating conditions is needed. In the present work, we propose metal–organic

[a] *School of Physics, Indian Institute of Science Education and Research Thiruvananthapuram, Vithura, Thiruvananthapuram, Kerala 695551, India. E-mail: shaiju@iisertvm.ac.in*
[b] *School of Chemistry, Indian Institute of Science Education and Research Thiruvananthapuram, Vithura, Thiruvananthapuram, Kerala 695551, India*
[c] *Center for Advanced Materials Research with International Engagement (CAMRIE), Indian Institute of Science Education and Research Thiruvananthapuram, Maruthamala PO, Vithura, Kerala, 695551 India*
† Electronic supplementary information (ESI) available. See DOI: https://doi.org/10.1039/d4lf00263f

© 2024 The Author(s). Published by the Royal Society of Chemistry

Open Access Article. Published on 02 October 2024. Downloaded on 2/4/2026 5:17:06 AM.
This article is licensed under a Creative Commons Attribution-NonCommercial 3.0 Unported Licence.

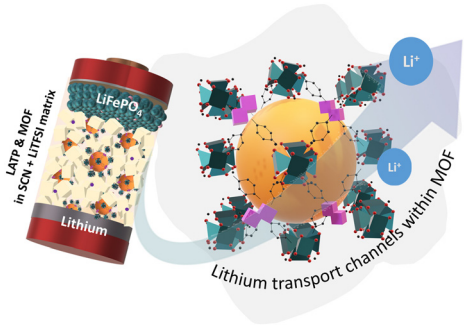

Scheme 1 Schematic representation of the MOF incorporated LATP electrolyte in an all-solid-state-battery (ASSB) configuration.

frameworks (MOFs) as polymer substitutes (Scheme 1) in solid electrolytes to achieve enhanced performance.

MOFs are not new to battery chemistry since they have applications in cathode additives, permselective separators, and fillers for polymer electrolytes.[9–11] The crystalline nature of MOFs can supply a distinct platform for the motion of ionic species in nano-porous space.[12,13] Further, MOFs act as single-ion conducting channels and enable fast conduction of Li ions.[14–16] Herein, we demonstrate MOFs as an effective substitute for polymer-based binders in solid-state electrolytes that ensure enhanced contact between electrodes and electrolytes, further leading to improved conductivity and overall cycling performance. We employ MOF-841 ($Zr_6O_4(OH)_4(MTB)_2(HCOO)_4(H_2O)_4$) as a filler, owing to its highly porous nature,[17,18] along with an LATP-based solid electrolyte. We show that with an appropriate blend of MOFs with LATP, enhanced performance could be achieved even with cold-pressing the pellet. Composite solid electrolytes (CSEs) composed of LATP ceramic particles and MOFs in a SCN–LiTFSI matrix are prepared, and their electrochemical properties are compared with CSEs fabricated using a PTFE binder.

As shown in Scheme 1, a full cell fabricated with an LATP–MOF composite solid electrolyte, lithium metal anode and $LiFePO_4$ cathode exhibits excellent electrochemical properties in terms of improved cycling and rate performance. Further, we have attempted to demonstrate an alternate conversion cathode using the electrolyte in a Li–Se all-solid-state battery configuration.

Experimental section

Citric acid monohydrate ($C_6H_8O_7{\cdot}H_2O$, ≥99.5%), nitric acid (HNO_3, 70%), titanium(IV) isopropoxide ($Ti\{OCH(CH_3)_2\}_4$, 99.999%), lithium nitrate ($LiNO_3$, 99.99%), aluminium nitrate nonahydrate ($Al(NO_3)_3{\cdot}9H_2O$, ≥98%), ammonium dihydrogen phosphate ($NH_4H_2PO_4$, 99.999%), succinonitrile ($C_4H_4N_2$), and lithium bis(trifluoromethane sulfonyl)imide (LiTFSI) were procured from Sigma Aldrich and used as such. Air-sensitive samples, such as lithium salts, were stored in a glove box to prevent moisture uptake. Zirconium metal–organic framework ($Zr_6O_4(OH)_4MTB_2(HCOO)_4(H_2O)_4$) MOF-841 with a surface area of 1067 $m^2\ g^{-1}$ and a pore size of 0.40 $cm^3\ g^{-1}$ was procured commercially from Nanoshel, UK and used as such.

Preparation of LATP sintered pellets by a sol–gel method

LATP was synthesised by a facile sol–gel method. All precursors were measured in stoichiometric amounts. In accordance with the calculations, an appropriate amount of $Ti\{OCH(CH_3)_2\}_4$ was added to 20 mL of deionised water to form a white $Ti(OH)_4$ precipitate. This precipitate was then filtered, washed and transferred into a beaker, to which a mixture of 10 mL deionised water and 15 mL HNO_3 was added at a rate of 100 mL min^{-1}. When a clear TiO^{2+} nitrate solution was formed, $C_6H_8O_7{\cdot}H_2O$ was added to stabilise the solution. While stirring, stochiometric amounts of $LiNO_3$ and $Al(NO_3)_3{\cdot}9H_2O$ were added to the solution. Subsequently, after the dissolution of the precursors, $NH_4H_2PO_4$ was added to the solution, and a sol was immediately formed. The stiff gel thus formed was dried at 80 °C for 24 h. The dried gel was sintered at 200 °C and 600 °C for 2 and 3 h, respectively. The powder obtained was ground, sieved and pressed into a pellet at a pressure of 70 MPa. These pellets were calcined at 850 °C for 5 h and ground to obtain LATP powder. LATP powder was later sieved using a sieve of mesh size 50 μm, and the obtained powder was used for preparing the cold-pressed pellets.

Preparation of SCN–LiTFSI-infused pellets

After heating succinonitrile (SCN) at 60 °C, lithium bis(trifluoromethanesulfonyl)imide (LiTFSI) was added and stirred till a uniform solution ($W_{SCN}:W_{LiTFSI}$ = 20 : 1) was formed. The cold-pressed pellets were prepared by mixing 200 mg of the as-synthesised LATP powder with 10 mg of PTFE and MOF and were pressed into pellets at a pressure of 70 MPa to obtain the three required combinations of the composite solid electrolyte. The pellets were dipped in the solution. Upon removing the dipped pellet from the hot plate, the solution hardened to form a thick gel-like substance. The dipped pellet was stored for 48 h at RT in a glove box prior to cell assembly.

Physicochemical characterisation

The phase purity of the LATP powder sample was analysed using a Bruker X-ray diffractometer (XRD) in the 2θ range of 15–80° equipped with a Cu-Kα source. The morphology of the cross-section of the pellet and its interfaces were examined using a field emission scanning electron microscope (Nova NanoSEM 450). Solid-state NMR (ssNMR) spectroscopy measurements were performed on a Bruker Avance Neo spectrometer functioning at a ^1H Larmor frequency of 500 MHz, corresponding to a ^7Li Larmor frequency of 194.43 MHz. All the samples were loaded in 3.2 mm zirconia rotors inside an argon-filled glove box to avoid moisture contact. ^7Li chemical shifts were referenced to LiCl at 0 ppm. One pulse experiment with a π/2 pulse width of 4.5 μs was used to perform ^7Li line shape measurements. X-ray photoelectron spectroscopy (XPS)

Open Access Article. Published on 02 October 2024. Downloaded on 2/4/2026 5:17:06 AM.
This article is licensed under a Creative Commons Attribution-NonCommercial 3.0 Unported Licence.

measurements were performed on an ESCA plus XPS spectrometer (Omicron Nanotechnology Ltd, Germany) equipped with monochromatic Mg-Kα (energy 1253.6 eV). Deconvolution of the peaks was carried out using CASA XPS software.

Electrochemical measurement

Commercial $LiFePO_4$ was used as a cathode active material for Li-ion battery studies. For the Li–Se system, a carbon selenium composite cathode was employed. The preparation procedure is detailed in the ESI.†

The cathodes for Li-ion and Li–Se cells were prepared by mixing the active materials *viz.* commercial $LiFePO_4$ and the carbon–Se cathode, respectively, in a 70 : 20 : 10 (wt%) ratio with carbon black and polyvinylidene fluoride (PVDF) in *N*-methyl-2-pyrrolidone (NMP) solvent to obtain a thick slurry. This slurry was then coated on aluminium foil and dried in a 60 °C furnace for 12 h. The dried electrode was then cut into discs of 11 mm diameter and incorporated in split cells (active material loading 2–3 mg cm^{-2}) with lithium metal as a counter electrode in an argon-filled glove box.

Electrochemical characterisation

A 2032-type coin cell comprising a 200 μm pellet placed between two stainless steel discs was assembled to estimate the ionic conductivity of the ceramic solid electrolyte. The ionic conductivity of all the combinations was analysed at different temperatures from 20 to 70 °C using electrochemical impedance spectroscopy (EIS). The EIS data measurements were performed using an Origa Flex-OGF500 potentiostat–galvanostat between 1 MHz and 100 MHz. The DC polarisation measurements were carried out using a Keithley 6430 source measure unit, which can measure current with 1 aA (10^{-18} A) sensitivity. The compatibility measurements of the solid electrolyte were carried out with a half cell (Li|SSE|LFP) at 24 h intervals for 10 days to obtain the Nyquist plot. Li plating and stripping studies were done in a symmetric cell (Li|SSE|Li) by applying a constant current of 0.1 mA cm^{-2}. The resulting overpotential *vs.* time data were recorded for 50 h. EIS measurements were performed to ensure that there was no internal cell shorting.

Moreover, the polarisation response was studied upon observing the variation in overpotential at a current density at 0.1 mA cm^{-2}. All-solid-state lithium batteries were assembled using $LiFe(PO_4)_3$/NC–Se as the working electrode along with an LATP combination as the ceramic solid electrolyte in between and metallic lithium as the counter electrode. It is also worth mentioning that no liquid electrolyte is involved in any of the studies presented in this work.

Results and discussion

The first step of synthesising LATP is detailed in the ESI† and schematically represented in Fig. 1a. The powder X-ray diffraction (XRD) pattern of the sample upon crushing the pellet is depicted in Fig. 1b. The peaks match well with the LATP reference data (00-035-0754). A small peak attributed to $AlPO_4$ impurity is also noticed. The scanning electron microscopy (SEM) images of the pellet cross section and its packing are shown in Fig. 1c and d. The digital photograph is provided as the inset of Fig. 1d. The ionic conductivity of the pellet measured by carrying out electrochemical impedance spectroscopy (EIS) turns out to be 22.1 mS cm^{-1} at RT. The recorded Nyquist plot is presented as the inset of Fig. 1e. The values agree with the literature,[19] and hence, the LATP pellets are crushed and used for further studies.

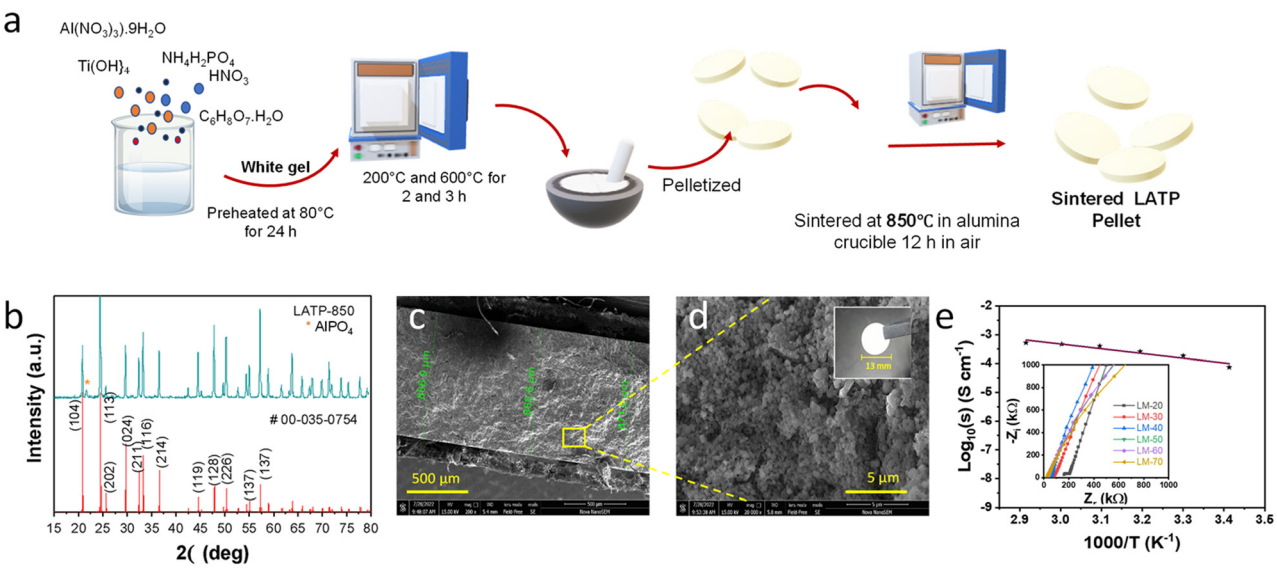

Fig. 1 (a) Schematic representation of the synthesis of LATP pellets. (b) XRD patterns, (c) cross-section SEM image, and (d) SEM image of an LATP pellet. Inset of (d) shows a digital photograph of the pellet. (e) Ionic conductivity plot of LATP.

© 2024 The Author(s). Published by the Royal Society of Chemistry

Open Access Article. Published on 02 October 2024. Downloaded on 2/4/2026 5:17:06 AM.
This article is licensed under a Creative Commons Attribution-NonCommercial 3.0 Unported Licence.

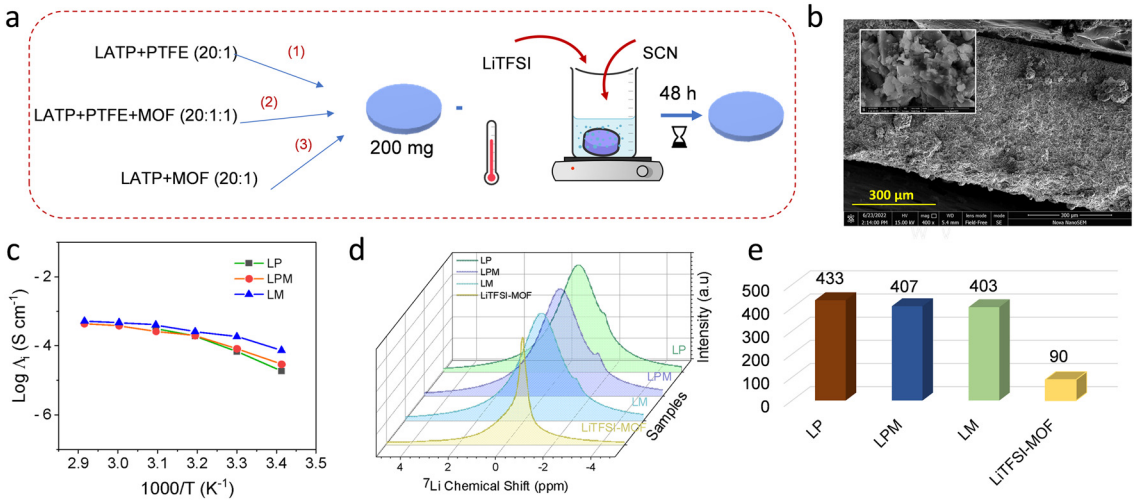

Fig. 2 (a) Schematic of the preparation of the solid electrolyte. (b) The cross-section SEM image of the pellet post-SCN + LiTFSI incorporation. Inset of (b) shows magnified image of the cross-section. (c) Ionic conductivity plot for the three different compositions. (d) ^{7}Li NMR studies of the pellets and the corresponding (e) histogram of their FWHM.

Three different composites were prepared and dipped in succinonitrile (SCN) with 5% LiTFSI for 48 h, namely LATP + PTFE (LP), LATP + PTFE + MOF (LPM) and LATP + MOF (LM). The pellets' surface was scrubbed gently to remove excess plasticiser before further studies (Fig. 2a). The SEM image of the pellet cross-section and the corresponding EDX spectra of the compositions before dipping in the plasticiser are provided in Fig. S1.† The pellet thickness was approx. 600 to 700 µm, as shown in Fig. 2b, and the inset shows the compact packing of the composite electrolyte upon plasticiser incorporation. The ionic conductivity of all three samples was measured (Fig. 2c), and it was found that LM has the highest conductivity of 24.7 mS cm^{-1} compared to all the other samples (15.4 mS cm^{-1} for LP) at RT. The Nyquist plots used for plotting the Arrhenius plots are presented in Fig. S2,† and the estimated activation energy is also presented. The MOF incorporation and PTFE replacement are shown to decrease the activation energy from 0.32 to 0.13 eV. This is the first noticeable evidence of a performance enhancement with MOF incorporation during our studies. NMR studies were conducted to substantiate the results and understand the ion diffusivity. The narrowing of the FWHM is associated with improved ion mobility in the electrolyte matrix.[20,21] Upon carrying out ^{7}Li NMR measurements (Fig. 2d), we notice a drop in FWHM from 433 to 403 a.u. (Fig. 2e). These measurements have proven that MOFs are cation carriers. The intrinsically ordered pore structure of MOFs with a high specific surface area aids efficient pathways for ion migration and facilitates efficient loading of Li-ion-containing electrolytes into their inner spaces.[22] Also, the Lewis acid nature of MOFs helps localise anions and increases Li ion mobility as witnessed by NMR studies.

To check if MOFs can address the issues associated with the interfacial reactions, particularly with LATP, we performed plating–stripping studies of Li|Li symmetric cells with the three test systems by assembling a split cell, as shown in Fig. 3a. The constant current measurements with 0.1 mA cm^{-2} for 30 min charge and discharge reveal that LM offers a stable overpotential of 77 mV (Fig. 3b–d). The histogram in Fig. 3e explicitly shows the overpotential trend. The increase in overpotential for the PTFE-containing LPM electrolyte reflects the passivating interfacial growth. The case of LP is even worse than LPM. MOFs can henceforth be used as substitutes for such passive binding agents. Not only does its porous structure help absorb the plasticiser, but also the Li transport through the channel paves the way for improved kinetics.[13] It is also worth mentioning that no surface modification was applied to SEs before full cell testing.

In an all-solid-state full-cell configuration, the ionic and electronic transport completely relies on solid–solid contact in all-solid-state batteries.[23,24] To further understand the overall performance of the electrolyte of our interest, cycling studies were carried out with full cells composed of LFP and metallic Li electrodes (Fig. 4a). All the electrochemical tests were carried out at room temperature. A comparison of the cycling profile is depicted in Fig. 4b. The studies demonstrate that apart from the LM containing full-cell offering an enhanced capacity of 138 mA h g^{-1}, compared to LPM, which delivers 111 mA h g^{-1}, there is a significant difference in their overpotentials.

It is worth mentioning that the pellets were prepared with similar mass loading and dipped in the plasticiser for equal time intervals. Even then, the LM electrolyte offered the least overpotential. For comparison, the overpotential at 70% of SoC is measured respectively for both electrolytes. The LM-containing cell has an overpotential of 100 mV and 230 mV at 25 and 70% SoC, respectively (Fig. 4b). This performance enhancement is purely due to the addition of the MOF. Further, the rate capability of the cells is studied, as shown in Fig. 4c. Again, the MOF containing LM cell outperforms its counterparts and offers the best rate capability, demonstrating 80 mA h g^{-1}

Open Access Article. Published on 02 October 2024. Downloaded on 2/4/2026 5:17:06 AM.
This article is licensed under a Creative Commons Attribution-NonCommercial 3.0 Unported Licence.

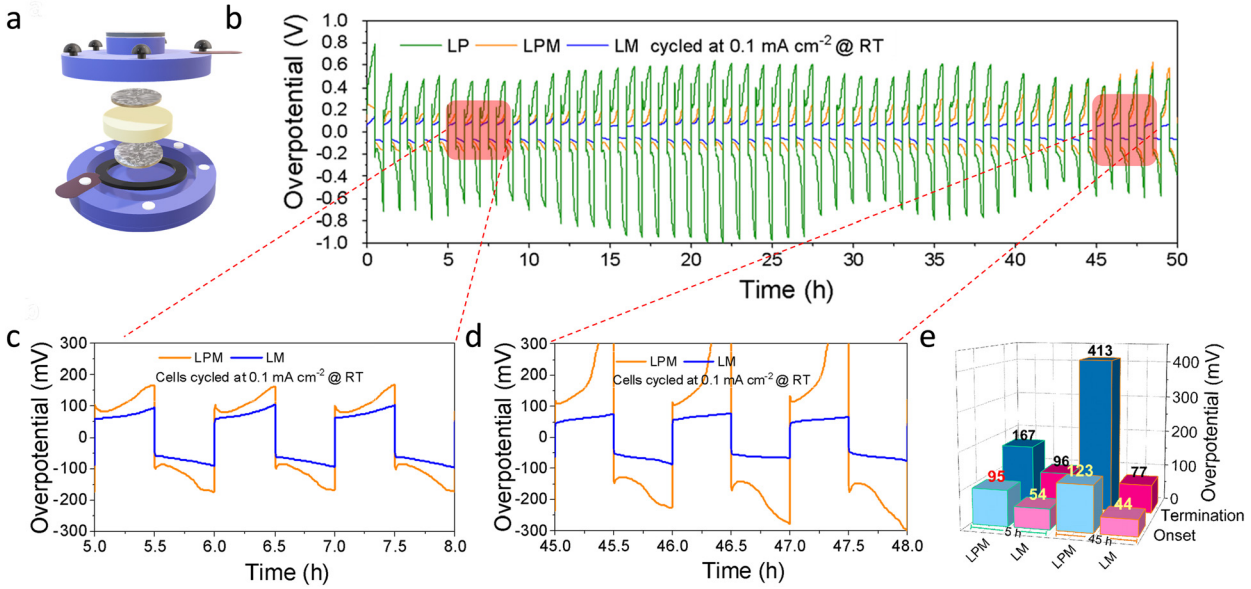

Fig. 3 (a) Schematic of the split cell used for constant current platting/stripping studies. (b) Overpotential *vs.* time plot is measured at RT, and the corresponding zoomed-in regions at (c) 5 to 8 h and (d) 45 to 48 h are highlighted. (e) Onset and termination overpotentials for LPM and LM at 5 h and 45 h represented as a histogram.

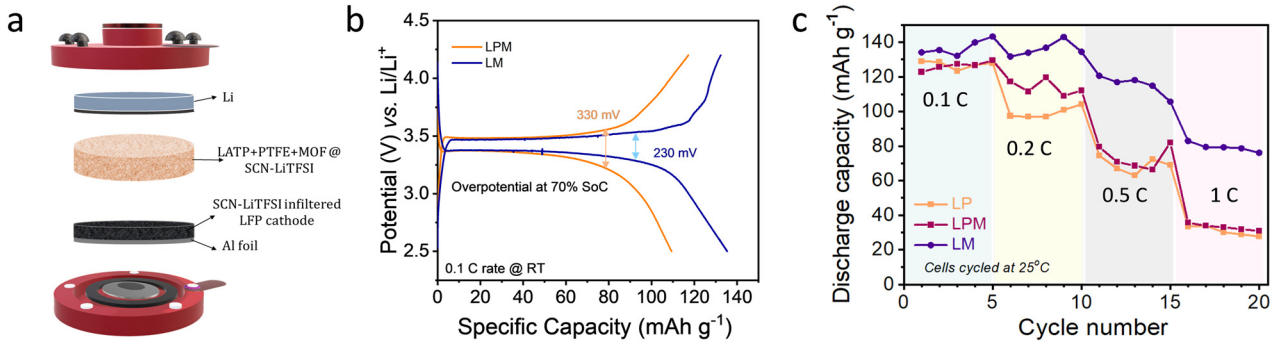

Fig. 4 (a) Pictographic representation of the full cell configuration with the LFP cathode and Li metal anode, (b) cycling profile of Li–LFP full cells with LPM and LM, and (c) rate capability studies of the Li–LFP cell with the three different electrolytes cycled at RT.

at a 1 C rate. Compared to the PTFE binders, which could presumably block ion transport, MOFs provide conduction channels that aid cycling at high current rates. The EIS of an LM containing full-cell after long cycling shows three semi-circles, possibly attributed to the grain boundary, LATP–MOF and electrode–electrolyte interface (Fig. S3†). Long-term cycling of lithium metal batteries strongly relies on the electrode–electrolyte interaction.[2] We also carried out long cycling studies for the LM containing full-cell at a 0.1 C rate, as shown in Fig. S4.† We observed that the cell delivered appreciable capacity retention and coulombic efficiency. Table S1† shows a comparison of the performance of our electrolyte with recent literature reports.[6,19,25–41]

To check if the MOFs are chemically stable upon cycling and to understand the nature of LATP, X-ray photoelectron spectroscopy (XPS) analyses were performed. Post-mortem XPS analysis of the materials reveals that Ti has undergone slight decomposition, resulting in Ti^{3+} and Ti^{4+} peaks (Fig. S6†). Had there been no decomposition, only the Ti^{4+} peak would have appeared.[42,43] Further, the Zr 2p peak is congruent to the XPS of MOF[44] and hence is stable upon cycling in the given potential window.

Lithium–chalcogen batteries with sulfur and selenium chemistries are also explored for achieving high energy density not just with liquid electrolytes but with solid electrolytes as well.[45–47] It is noteworthy that the formation and dissolution of polyselenides, which are a serious issue in Li–chalcogen systems using liquid electrolytes, are mitigated with the direct conversion mechanism in the solid-state configuration. Hence, to further expand the scope of the proposed electrolyte candidate, we carried out preliminary studies of lithium–selenium full cells in a coin cell configuration. The cathodic peak around 1.5 V and the anodic peak around 2.4 V (*vs.* Li) is attributed to the conversion of Se to Li_2Se and *vice versa*. The

© 2024 The Author(s). Published by the Royal Society of Chemistry

Open Access Article. Published on 02 October 2024. Downloaded on 2/4/2026 5:17:06 AM. This article is licensed under a Creative Commons Attribution-NonCommercial 3.0 Unported Licence.

all-solid-state Li–Se cell delivered a capacity of 375 mA h g^{-1} at a 0.1 C rate with appreciable stability (Fig. S7†). A comparable cycling profile and capacity are reported for an all-solid-state Li–Se battery fabricated by using a composite selenium cathode, a Li–In anode, and a Li_6PS_5Cl solid-state electrolyte.[48]

As emphasized in the previous discussion, the primary advantage of these electrolytes is the ease of preparation. Additionally, the Lewis acidic sites on the MOF surfaces serve as strong attraction sites for anions, promoting higher Li-ion mobility. We further envisage evaluating the cell performance under high-pressure conditions and improving the kinetics of ion transport and diffusion. To summarise, we studied the effect of MOFs added as conductive enhancers to composite solid electrolytes (CSEs) composed of LATP ceramic particles, MOFs and PTFE binders in a SCN–LiTFSI matrix.

Conclusions

The morphology, conductivity, and electrochemical cycling of LATP and its composite combinations were explored well. Further, we fabricated a full cell and showed that the LATP–MOF composite solid electrolyte, with lithium metal as the anode and $LiFePO_4$ as the cathode, exhibits much improved electrochemical performance with discharge capacities of 138 mA h g^{-1} and 111 mA h g^{-1} at 0.1 and 0.5 C-rates, respectively. Optimisation studies involving the varying nature of MOFs, their cage structures, and the ceramic-to-MOF ratio are underway, and there is a wide scope for exploring the same. This proposed approach of using MOFs as conductivity boosters is not limited to the LATP system but will promote broader research into MOF-incorporated CSEs and further expand to other classes of electrolytes like sulfides and argyrodites. We believe that the implication of MOFs will occur in tandem with progress in the broader solid electrolyte field.

Data availability

Data for the article "Metal–organic frameworks as conductivity enhancers for all-solid-state lithium batteries" are available at Open Science Forum at Shaijumon, M. M. (2024, July 19). Solid-state battery. Retrieved from **https://osf.io/4wpts/**.

Conflicts of interest

There are no conflicts to declare.

Acknowledgements

MMS acknowledges the financial support from the Department of Science & Technology, Ministry of Science & Technology, Govt. of India, through DST-IISER Thiruvananthapuram Integrated Clean Energy Material Acceleration Platform (IC-MAP) [DST/TMD/IC-MAP/2K20/01].

Notes and references

1 A. K. Nayak, B. Ganguli and P. M. Ajayan, *Energy Rep.*, 2023, **9**, 3508.
2 S. Sunny, S. Suriyakumar, A. S. Sajeevan and M. M. Shaijumon, *JPhys Energy*, 2024, **6**, 022004.
3 C. Yada, C. E. Lee, D. Laughman, L. Hannah, H. Iba and B. E. Hayden, *J. Electrochem. Soc.*, 2015, **162**, A722.
4 S. Song, N. Hu and L. Lu, *Chem. Commun.*, 2022, **58**, 12035.
5 P. Aswathy, S. Suriyakumar, S. A. Kumar, M. S. Oliyantakath Hassan, V. Vijayan and M. M. Shaijumon, *ACS Appl. Energy Mater.*, 2022, **5**, 12592.
6 Q. Wang, A. Yang, J. Ma, M. Yao, S. Geng and F. Liu, *Electrochim. Acta*, 2023, **467**, 143138.
7 Z. Yang, H. Yuan, C. Zhou, Y. Wu, W. Tang, S. Sang and H. Liu, *Chem. Eng. J.*, 2020, **392**, 123650.
8 W. Cao, Y. Yang, J. Deng, Y. Li, C. Cui and T. Zhang, *Mater. Today Energy*, 2021, **22**, 100875.
9 S. Suriyakumar, A. M. Stephan, N. Angulakshmi, M. H. Hassan and M. H. Alkordi, *J. Mater. Chem. A*, 2018, **6**, 14623.
10 S. Suriyakumar, S. Gopi, M. Kathiresan, S. Bose, E. B. Gowd, J. R. Nair, N. Angulakshmi, G. Meligrana, F. Bella, C. Gerbaldi and A. M. Stephan, *Electrochim. Acta*, 2018, **285**, 355.
11 L. Yu, T. Pang, Y. Li, H. Zhang, Y. Yu and N. Zhang, *Mater. Lett.*, 2024, **365**, 136416.
12 R. Zhao, Z. Liang, R. Zou and Q. Xu, *Joule*, 2018, **2**, 2235.
13 J. Zhang, Y. Wang, Q. Xia, X. Li, B. Liu, T. Hu, M. Tebyetekerwa, S. Hu, R. Knibbe and S. Chou, *Angew. Chem., Int. Ed.*, 2024, e202318822.
14 H. Yang, B. Liu, J. Bright, S. Kasani, J. Yang, X. Zhang and N. Wu, *ACS Appl. Energy Mater.*, 2020, **3**, 4007.
15 S. Kim, H. Jamal, F. Khan, A. Al-Ahmed, M. M. Abdelnaby, A. Al-Zahrani, S.-E. Chun and J. H. Kim, *J. Mater. Chem. A*, 2024, **12**, 10942.
16 J. Li, F. Xie, W. Pang, Q. Liang, X. Yang and L. Zhang, *Sci. Adv.*, 2024, **10**, 3925.
17 L. Xia and F. Wang, *Inorg. Chim. Acta*, 2016, **444**, 186.
18 H. Furukawa, F. Gándara, Y. B. Zhang, J. Jiang, W. L. Queen, M. R. Hudson and O. M. Yaghi, *J. Am. Chem. Soc.*, 2014, **136**, 4369.
19 R. DeWees and H. Wang, *ChemSusChem*, 2019, **12**, 3713.
20 X. Zhang and H. Huo, *Magn. Reson. Lett.*, 2021, **1**, 142.
21 V. Epp, Q. Ma, E. M. Hammer, F. Tietz and M. Wilkening, *Phys. Chem. Chem. Phys.*, 2015, **17**, 32115.
22 G. H. Kim, J. Jang and J. Kang, *ACS Appl. Mater. Interfaces*, 2024, **16**, 36479.
23 Q. Zhao, S. Stalin, C. Z. Zhao and L. A. Archer, *Nat. Rev. Mater.*, 2020, **5**, 229.
24 S. A. Pervez, M. A. Cambaz, V. Thangadurai and M. Fichtner, *ACS Appl. Mater. Interfaces*, 2019, **11**, 22029.
25 V. Siller, A. Morata, M. N. Eroles, R. Arenal, J. C. Gonzalez-Rosillo, J. M. López Del Amo and A. Tarancón, *J. Mater. Chem. A*, 2021, **9**, 17760.
26 E. Zhao, F. Ma, Y. Guo and Y. Jin, *RSC Adv.*, 2016, **6**, 92579.
27 Y. Li and H. Wang, *Ind. Eng. Chem. Res.*, 2021, **60**, 1494.

© 2024 The Author(s). Published by the Royal Society of Chemistry

Open Access Article. Published on 02 October 2024. Downloaded on 2/4/2026 5:17:06 AM.
This article is licensed under a Creative Commons Attribution-NonCommercial 3.0 Unported Licence.

28 L. Liu, L. Chu, B. Jiang and M. Li, *Solid State Ionics*, 2019, **331**, 89.
29 Z. Y. Kou, Y. Lu, C. Miao, J. Q. Li, C. J. Liu and W. Xiao, *Rare Met.*, 2021, **40**, 3175.
30 Y. Liu, J. Liu, Q. Sun, D. Wang, K. R. Adair, J. Liang, C. Zhang, L. Zhang, S. Lu, H. Huang, X. Song and X. Sun, *ACS Appl. Mater. Interfaces*, 2019, **11**, 27890.
31 Y. Huang, Z. Zhang, H. Gao, J. Huang and C. Li, *Solid State Ionics*, 2020, **356**, 115437.
32 S. Sharma, M. D. Singh and A. Dalvi, *J. Energy Storage*, 2022, **49**, 104178.
33 Q. Cheng, A. Li, N. Li, S. Li, A. Zangiabadi, T. De Li, W. Huang, A. C. Li, T. Jin, Q. Song, W. Xu, N. Ni, H. Zhai, M. Dontigny, K. Zaghib, X. Chuan, D. Su, K. Yan and Y. Yang, *Joule*, 2019, **3**, 1510.
34 F. Yang, Q. Liu, W. Xie, P. Xie, J. Shang and X. Shu, *Polymer*, 2022, **14**, 1274.
35 S. Wang, S. Li, B. Wei and X. Lu, *J. Electrochem. Soc.*, 2020, **167**, 100528.
36 K. Waetzig, A. Rost, C. Heubner, M. Coeler, K. Nikolowski, M. Wolter and J. Schilm, *J. Alloys Compd.*, 2020, **818**, 153237.
37 J. Li, X. He, W. Yuan, M. Yu, X. Wang, T. Zhang, L. Luan, Y. Ding and H. Sun, *ACS Appl. Energy Mater.*, 2024, **7**, 3484.
38 C. J. Park, S. Na, H. G. Park and K. Park, *ACS Appl. Mater. Interfaces*, 2023, **15**, 26985.
39 H. Y. Xu, G. T. Fei, S. H. Xu, W. C. Chen, S. J. Li, X. F. Li and H. M. Ouyang, *Solid State Ionics*, 2024, **412**, 116603.
40 Y. Cho, A. Le Mong, H. A. Hoang and D. Kim, *J. Energy Storage*, 2024, **92**, 112295.
41 H. Anwar, H. Bin Shahid, H. Ahmad, K. Nasir, Z. Ali and G. Ali, *Energy Storage*, 2024, **6**, e628.
42 Z. Lu, Z. Chen, M. Wang, Y. Wan, J. Yan, S. Chen, Y. Shen, Z. Yan and D. Wang, *ACS Appl. Energy Mater.*, 2023, **6**, 2541.
43 C. Huang, Z. Li, S. Duan, S. Xie, S. Yuan, S. Hou, G. Cao and H. Jin, *J. Power Sources*, 2022, **536**, 231491.
44 Y. Wang, L. Li, P. Dai, L. Yan, L. Cao, X. Gu and X. Zhao, *J. Mater. Chem. A*, 2017, **5**, 22372.
45 J. M. Sudharma, S. K. Jayaprakash, S. Suriyakumar, B. Rajbongshi and M. M. Shaijumon, *Energy Adv.*, 2024, **3**, 215.
46 G. L. Xu, H. Sun, C. Luo, L. Estevez, M. Zhuang, H. Gao, R. Amine, H. Wang, X. Zhang, C. J. Sun, Y. Liu, Y. Ren, S. M. Heald, C. Wang, Z. Chen and K. Amine, *Adv. Energy Mater.*, 2019, **9**, 1802235.
47 Y. Li, Z. Li, L. Yue, Y. Zhang, S. Liu, Y. Niu, S. Zhang and M. Xu, *Adv. Sci.*, 2023, **10**, 2206962.
48 C. Li, R. Liu, S. Zhang, Q. Li, C. Wang, Z. Zhang, C. Wang, L. Yin and R. Wang, *Chin. Chem. Lett.*, 2023, **34**, 108083.

© 2024 The Author(s). Published by the Royal Society of Chemistry